Journal of the European Ceramic Society 22 (2002) 2527–2535

www.elsevier.com/locate/jeurceramsoc

Thermal stability of in situ formed Si_3N_4–Si_2N_2O–TiN composites

Ren-Guan Duan, Gert Roebben*, Jef Vleugels, Omer Van der Biest

Department of Metallurgy and Materials Engineering, K.U. Leuven, Kasteelpark Arenberg 44, B-3001 Heverlee, Belgium

Received 10 October 2001; accepted 14 April 2002

Abstract

To investigate the potential of in situ formed Si_3N_4–Si_2N_2O–TiN composites, mixtures of Si_3N_4 with TiO_2 and TiN powders were hot-pressed. Seven different compositions were successfully densified at 1650 °C resulting in various Si_3N_4-, Si_2N_2O- and TiN-volume fractions. The effect of elevated temperatures (up to 1400 °C) on the microstructure of these composites was explored, using internal friction measurements with the impulse excitation technique (IET) and high temperature X-ray diffraction (HTXRD). The bulk microstructure of the tested composites is stable up to 1400 °C, both with respect to the crystalline phase composition, as well as the intergranular glass phases. Sample surfaces are affected due to the reducing atmosphere in which IET and HTXRD tests are performed (N_2 or vacuum). This involves the silicon oxynitride phase, which is not stable at temperatures above 1300 °C in the presence of a substantial amount of amorphous intergranular phase. Based on the results of indentation toughness and hardness tests, a high-Si_2N_2O/high-TiN/β-Si_3N_4 is selected as most promising for further development.

Keywords: Grain boundaries; Mechanical properties; Mechanical spectroscopy; Si_3N_4

1. Introduction

Silicon nitride-based materials have promising high-temperature properties such as strength, creep resistance, and oxidation resistance. However, the presence of an intergranular glass phase can be detrimental for these high-temperature properties. Post-sinter heat treatments are often used to devitrify the glass, resulting in Si_3N_4-based composite microstructures of chemically compatible crystalline phases.[1–3]

A particular example of such secondary phase is silicon oxynitride (Si_2N_2O), which is also encountered in its Al-substituted form 'O-sialon' (a solid solution of Si_2N_2O and Al_2O_3, represented by the formula: $Si_{2-x}Al_xO_{1+x}N_{2-x}$, with x less than 0.2 at 1800 °C).[4] Although Si_2N_2O was already discovered in 1926, information on the mechanical, thermal and thermodynamic properties of Si_2N_2O (and the O-sialon) phase is scarce.[5] Like Si_2N_2O, O-sialon shows a needle or plate-like grain morphology,[6–9] hence its potential for toughening silicon nitride-based ceramics through the mechanism of crack wake bridging.

The incorporation of TiN particles in the silicon nitride microstructure is also expected to increase its toughness. Moreover, the hardness and electrical conductivity of TiN should bring about a material which is at the same time wear resistant and (electro-) machinable.[10–13]

Given the earlier observations, and following-up on a prior study of the effect of Ti-additives on the properties of Si_3N_4-based ceramics,[14] this paper presents the results of a first exploration of the processing and thermal stability of in-situ formed Si_3N_4–Si_2N_2O–TiN ceramic composites. Internal friction tests with the impulse excitation technique (IET), and high temperature X-ray Diffraction (HTXRD) are used to assess the intergranular glass phase and the crystalline phases in these materials at elevated temperature.

2. Experimental procedure

2.1. Sample preparation

Seven different silicon nitride-based composites are prepared (Table 1). Two of these ceramics (SN-Al4 and SN-Y2Al4TiN2) have previously been discussed by Duan et al.[14] The starting powders used are Si_3N_4

* Corresponding author. Tel.: +32-16-321-192; fax: +32-16-321-992.

E-mail address: gert.roebben@mtm.kuleuven.ac.be (G. Roebben).

0955-2219/02/$ - see front matter
PII: S0955-2219(02)00110-3

Table 1
Composition of the starting powder mixtures (in wt.%) including Al_2O_3 pick-up from ball milling

	SN-Y2Al4TiN2	SN-Y2Al3TiN2	SN-Al5TiN4	SN-Al6TiO4	SN-Y6TiO4	SN-Y6TiO20	SN-Al4
Si_3N_4	92	96	96	96	90	74	96
Y_2O_3	2	2	0	0	6	6	0
TiO_2	0	0	0	4	4	20	0
TiN	2	2	4	0	0	0	0
Al_2O_3	4	0	0	0	0	0	4
Al_2O_3[a]	0.5	3.0	5.1	6.3	0	0	0.3

[a] The amount of Al_2O_3 pick-up during alumina ball milling.

(HCST grade LC12-SX, 97% α-Si_3N_4, submicron particle size, 1.8–2.1 wt.% oxygen), TiO_2 (2 micron, >99% rutile, Johnson Matthey Company), Al_2O_3 (Baikowski grade SM8, 95% α, submicron particle size), TiN (Ceramyg, France, submicron particle size), and Y_2O_3 (Aldrich Chemical Company, 99.99% pure). Powder mixtures were prepared by ball-milling for 4 h in isopropanol (Retsch B.V., the Netherlands), either with alumina balls in an alumina vessel or with sialon balls in a sialon vessel. The Al_2O_3 pick-up during alumina ball milling was assessed with XRF (Philips, PW2400 X-ray spectrometer, The Netherlands), using a calibration curve based on measurements on powder mixtures of Al_2O_3 and α-Si_3N_4. The nominal composition of the powder mixtures and the Al_2O_3 pick-up from ball milling is listed in Table 1. Different amounts of Al_2O_3 pick-up originate from different rotation speeds during ball milling.

After evaporation of the isopropanol by means of a rotating evaporator, the dry powder mixture was put in a graphite container, coated with boron nitride. The samples were cold pressed at 30 MPa and subsequently hot-pressed in a KCE furnace (W100/150–2200–50LAX, KCE Sondermaschinen, Germany) under vacuum (0.1 Pa) at 1650 °C for 1 h under a mechanical load of 20 MPa. The heating rate was 50 °C/min, the cooling rate 20 °C/min.

2.2. Materials characterisation

All seven of the powder mixtures (Table 1) were successfully densified after the 1650 °C hot-press cycle. This justified an initial screening of their microstructure and mechanical properties, using techniques requiring relatively small amounts of test material, such as XRD, SEM and IET.

Rectangular beam-like samples were tested with the IET to determine their elastic and damping properties. The E-modulus was calculated from the bending vibration frequency f_b according to the equation proposed in ASTM E 1876–99: $E = 0.9465(m(f_b)^2/b)(L^3/t^3)T_1$, with m, L, b and t, the sample weight, length, width, and thickness, respectively. T_1 is a correction factor, depending on the Poisson's ratio and the thickness/length ratio.[15] Reported E-modulus uncertainties are the result of an error propagation analysis based on the uncertainties of the experimental measurement of dimensions and resonance frequency.

For high temperature IET-tests, the samples were suspended in the nodes of their first bending vibration mode, and measured in an IET-furnace with graphite heating elements (HTVP 1750-C, IMCE, Diepenbeek, Belgium) in a nitrogen atmosphere. Before heating, the furnace was purged three times with N_2 (L'air Liquide dry nitrogen with 10 ppm H_2O). The sample is heated up to and cooled down from 1400 °C at a rate of 2 °C/min. Impulse excitations are given to the sample every 60 s. The resulting vibration signals, captured with a microphone are analysed with the Resonance Frequency and Damping Analyser (RFDA, IMCE, Diepenbeek, Belgium) as described elsewhere.[16] The internal friction is calculated as $Q^{-1} = k/(\pi f_b)$, where k is the exponential decay parameter of the amplitude of the bending vibration component f_b.

High temperature X-ray diffraction was performed on a θ–θ diffractometer (3003-TT, Seifert, Ahrensburg, Germany) using Cu-K_α radiation (40 kV, 30 mA). A parabolic multilayer mirror transforms the divergent incident beam into a parallel beam, which is required to eliminate misalignment effects due to thermally induced sample position change during high temperature tests. A long 0.4° collimator in front of the scintillation detector increases angular resolution.

The high temperature tests were done in an X-ray furnace (HDK2.4, Johanna Otto, Hechingen, Germany). Tests were performed either in a flow of nitrogen gas (150 ml/min, L'air Liquide purified nitrogen with 5 ppm H_2O, 3 ppm O_2 and 1 ppm H_2) using a molybdenum heating element, or in vacuum ($<10^{-4}$ Pa measured at the furnace-pump connection) using a tantalum heating element. The heating elements essentially consist of a metal sheet, which is rolled in to a near-cylinder of nominally 20 mm diameter. The cylinder is left open over an angle of 60°, providing a window through which

X-rays have access to the surface of the sample positioned along the central axis of the cylinder. To improve the homogeneity of the temperature of the sample in the region irradiated by the X-rays, heating elements were prepared longer (26 mm) than the standard length (22 mm). Temperature is measured with a WRe thermocouple touching the sample in the X-ray irradiated zone of the sample surface. For each sample, consecutive diffraction spectra were acquired at room temperature, 500, 700, 900, 1000, 1100, 1200, 1300, and 1400 °C. Heating and cooling rate between two measuring temperatures was 30 °C/min. Data were obtained in a 2θ range from 10° to 45° (step width = 0.04°, measuring time = 1 s/step).

The hot-pressed silicon nitride based ceramics were polished, coated with carbon, and observed with a scanning electron microscope (SEM; XL30 FEG, Philips). Semi-quantitative electron probe microanalysis (EPMA) was performed on a Jeol JXA 733 Superprobe using an energy dispersive X-ray spectroscopy (EDS) analysis system (Tracor Northern).

Vickers hardness, H_V, was measured on a Zwick hardness tester with an indentation load of 10 kg. The indentation toughness, K_{Ic}, was obtained with the Vickers indentation technique, based on the crack length measurement of the radial crack pattern. The indentation K_{Ic} values were calculated using the formula: $K_{Ic} = 0.016(E/H_v)^{1/2}(P/(c^{3/2}))$, where E is the elastic modulus, H_V the hardness, P the indentation load, and c the radial crack length.[17] The reported K_{Ic} and H_V values are the mean of 10 measurements. The reported uncertainties are the standard deviations for these measurements.

3. Results

3.1. Microstructure

The results of the room temperature diffraction analysis are summarised in Table 2. No distinction is made at this point between Al-substituted or pure silicon (oxy-)nitride. The assumption is made that the presence of Al in the powder mixture automatically results in Al-substituted α-sialon, β-sialon or O-sialon rather than the pure silicon (oxy-)nitride phases. XRD-data and EDS aid in the identification of the constituent phases in the different ceramic grades on back-scattered-electron micrographs, as shown in Fig. 1 for four selected ceramics, SN-Y2Al4TiN2, SN-Al5TiN4, SN-Al6TiO4, and SN-Y6TiO20. EDS identifies the bright equiaxial grains in the SN-Y2Al4TiN2 ceramic (Fig. 1a) as TiN. The size of the white TiN grains is not uniform in the SN-Al5TiN4 ceramic (Fig. 1b), while it is uniform in the SN-Al6TiO4 ceramic (Fig. 1c). The darkest grains are identified as silicon oxynitride from their elongated morphology, volume fraction (as estimated from XRD-results), and lack of brightness (Si_2N_2O is the lightest of the major phases). There is a larger content of O-sialon in the SN-Al6TiO4 ceramic (Fig. 1c) than in the SN-Al5TiN4 ceramic (Fig. 1b). A large amount of TiN exists in the SN-Y6TiO20 ceramic (Fig. 1d) corresponding with the elevated TiO_2-content of the powder mixture.

HTXRD tests provide a unique in situ picture of the microstructural changes with temperature. One particular difficulty in the interpretation of HTXRD spectra of multi-phase materials is the phase-dependent shift of the peak positions due to the thermal expansion of the crystal structure. The average thermal expansion coefficient of TiN is, e.g. much larger (8×10^{-6}/°C) than that of Si_3N_4 (3×10^{-6}/°C). Moreover, the thermal expansion coefficient is also (hkl)-dependent.

The HTXRD results reveal the thermal stability of the α-sialon (or α-Si_3N_4), β-sialon (or β-Si_3N_4), and TiN phases up to 1400 °C. From the HTXRD spectra it appears however that silicon oxynitride (O-sialon or Si_2N_2O) is not stable up to 1400 °C in all of the composites. In the SN-Y2Al4TiN2 and SN-Y2Al3TiN2 ceramics, the O-sialon phase is present in the XRD spectra taken from room temperature up to 1300 °C. At more elevated temperatures, the O-sialon peaks decrease in intensity (when tested in nitrogen) or disappear (when tested in vacuum). Fig. 2a demonstrates the latter case, and indicates the appearance of an Y-silicate phase. EPMA results reveal the Y_2SiO_5 stoichiometry of the silicate grains.

Table 2
Crystalline phases in the different ceramic grades, as identified from XRD-spectra, SEM–EDS and EPMA analysis (+++: major phase, ++: important phase, +: minor phase, –: phase absent)

Ceramic grade	α-Si_3N_4 or α-sialon	β-Si_3N_4 or β-sialon	Si_2N_2O or O-sialon	TiN
SN-Y2Al4TiN2	++	+++	+	+
SN-Y2Al3TiN2	++	+++	+	+
SN-Al5TiN4	++	+++	++	+
SN-Al6TiO4	–	+++	++	+
SN-Y6TiO4	+++	+++	++	+
SN-Y6TiO20	+	++	+++	++
SN-Al4	–	+++	+	–

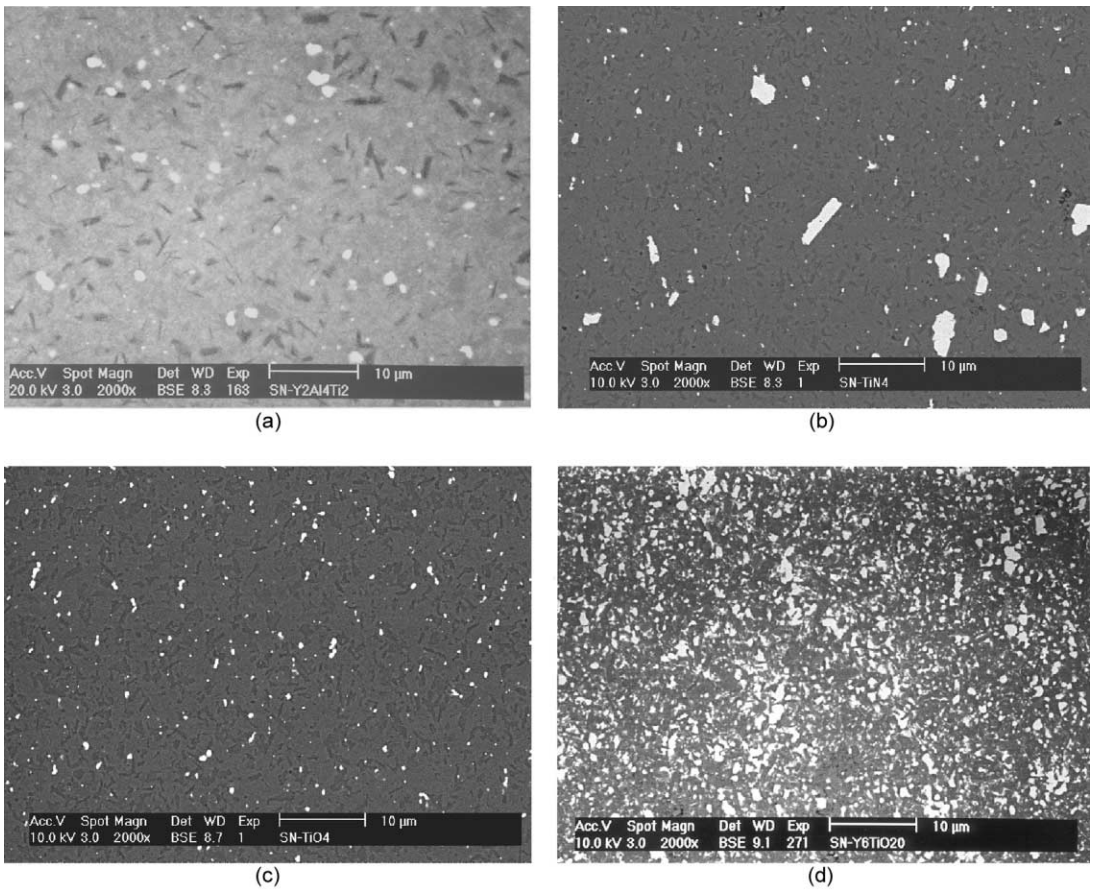

Fig. 1. Back-scattered electron images of four typical ceramics, (a) SN-Y2Al4TiN2, (b) SN-Al5TiN4, (c) SN-Al6TiO4, (d) SN-Y6TiO20.

Since XRD with Cu-K_α radiation is only penetrating the ceramic sample over about 30 μm, it was verified whether this observation is due to bulk phenomena, or whether it is a surface effect. After cooling, new XRD spectra were taken. Initial grinding down the outer surface layer easily removed the Y_2SiO_5 phase from the spectrum, but failed to make the O-sialon phase reappear. The silicon oxynitride phase volume fraction however is unaffected in the core of the 1 mm thick sample, as deduced from the XRD-spectrum taken after removing half the sample's thickness.

Fig. 2b illustrates the stability of the Si_2N_2O phase in the SN-Y6TiO20 material. Nevertheless, also in this material a surface layer is forming at elevated temperature. In this layer are recognised a Mo (originating from the heating element), and a (Y,Si)-phase. The stoichiometry of this phase was assessed with EPMA, but the phase with an uncommon 3/1 Y/Si ratio could not be identified.

3.2. Internal friction and mechanical properties

When heating up, the internal friction curves of the SN-Al5TiN4, SN-Al6TiO4, SN-Y6TiO4, SN-Y6TiO20, and SN-Al4 ceramics essentially follow an exponentially increasing trend, unlike the internal friction curves of the SN-Y2Al4TiN2 (previously reported by Duan et al.)[14] and SN-Y2Al3TiN2 ceramics (Fig. 3a) in which appears a large internal friction peak. Since the temperature at which the peak occurs is expected to be frequency-dependent, the resonant frequencies of the respective tested samples at room temperature are indicated in Fig. 3. When cooling from 1400 °C to room temperature, the internal friction peaks in the SN-Y2Al4TiN2 and SN-Y2Al3TiN2 ceramics are essentially unchanged (Fig. 3b). The *E*-modulus, Vickers hardness, and fracture toughness of the different composites are summarised in Table 3.

4. Discussion

4.1. Formation of Si_2N_2O and TiN during sintering

During heating to and at the densification temperature, the sintering additives react with the SiO_2-layer on the surface of the Si_3N_4 starting powder, to form an oxide liquid phase. Subsequently, the α-Si_3N_4 particles dissolve in this liquid phase, thus forming a silicon oxynitride liquid phase.[18,19] Local supersaturation leads to

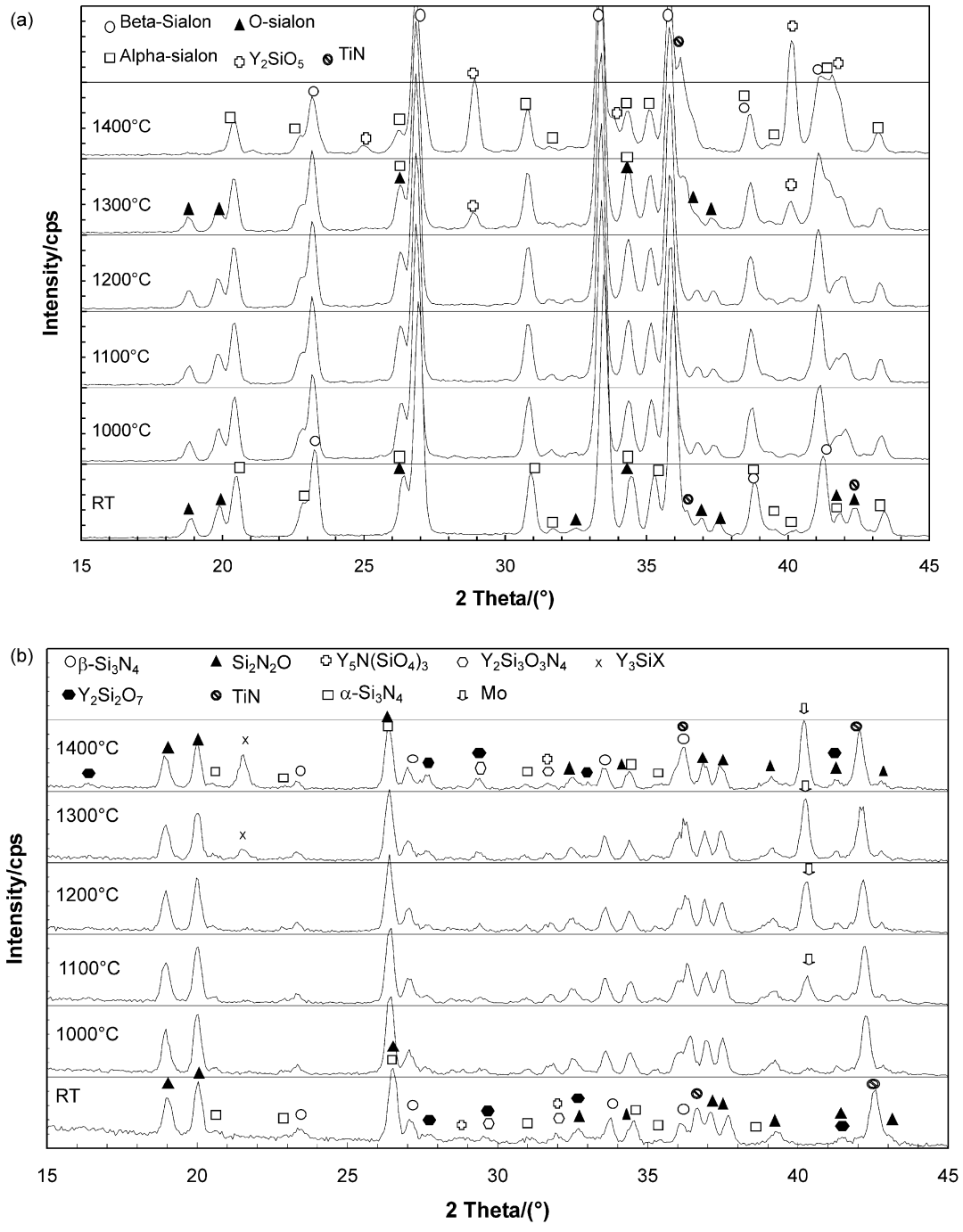

Fig. 2. High-temperature X-ray diffraction figs. of two typical ceramics, (a) SN-Y2Al4TiN2 measured in vacuum, (b) SN-Y6TiO20 measured in nitrogen.

reprecipitation of β-Si_3N_4 and/or silicon oxynitride grains.[6] Upon cooling, the amorphous phase solidifies, and devitrifies partially or totally. The remainder will constitute the intergranular glass phase. From the composition, density and microstructure of the sintered Si_3N_4–Si_2N_2O–TiN composites, it appears that this well-established sequence of events is not suppressed when TiO_2 or TiN is added to the powder mixture.

The TiN phase in the sintered ceramics is either the same material as the one which was added as a powder, or the product of an in-situ reaction of the TiO_2-additives. At the densification temperature, TiO_2 indeed reacts with α-Si_3N_4 according to the following equation: $6TiO_2(s) + 2Si_3N_4(s) = 6TiN(s) + 6SiO_2(l) + N_2(g)$. The Gibbs free energy, ΔG°, of this reaction at 1650 °C is −277 kJ/mol.[20] In the composites containing 4 wt.% of

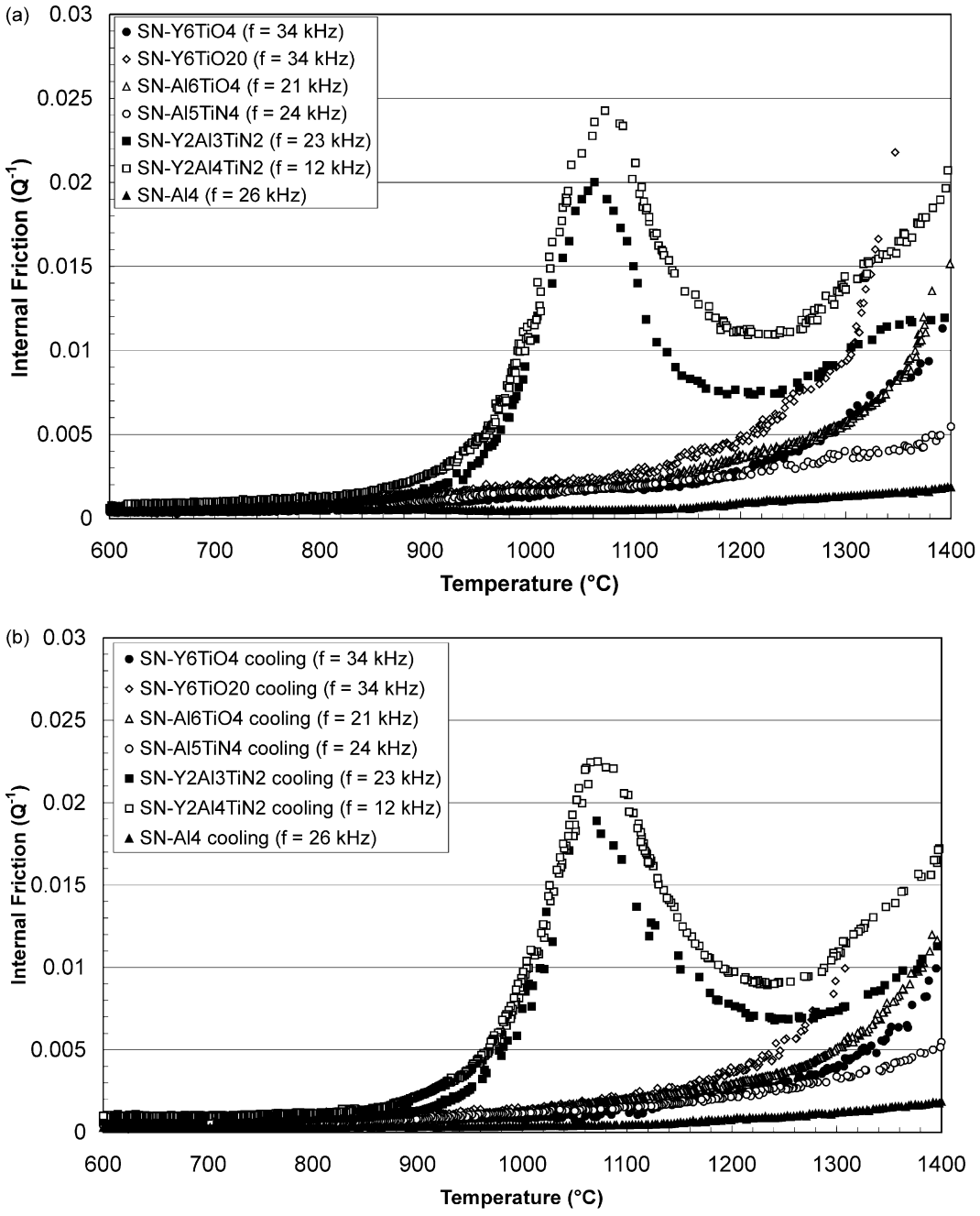

Fig. 3. The curves of internal friction (Q^{-1}) to the temperature for the ceramics SN-Y2Al4TiN2, SN-Y2Al3TiN2, SN-Al5TiN4, SN-Al6TiO4, SN-Y6TiO4, SN-Y6TiO20, and SN-Al4, (a) in the heating process, (b) in the cooling process.

Table 3
Mechanical properties of the different ceramic grades

Ceramic grade	E (GPa)	H_{v10} (kg/mm^2)	K_{IC} (MPa/m$^{1/2}$)	Q^{-1} (1250 °C)
SN-Y2Al4TiN2	302±10	1641±18	5.0±0.1	0.0110
SN-Y2Al3TiN2	295±10	1611±23	4.8±0.2	0.0080
SN-Y6TiO20	253±10	1619±35	4.3±0.2	0.0074
SN-Al6TiO4	276±10	1532±27	4.2±0.2	0.0045
SN-Y6TiO4	292±10	1575±41	3.7±0.3	0.0040
SN-Al5TiN4	290±10	1635±37	2.9±0.1	0.0030
SN-Al4	305±10	1618±18	2.6±0.1	0.0010

Ti-additives, it can be clearly seen how the in-situ formed TiN is more homogeneously dispersed and uniform in size and shape when compared to the TiN phase in the materials sintered with TiN additives (Fig. 1b and c).

4.2. Interpretation of the internal friction observations

An internal friction peak is commonly observed when silicon nitride based ceramics are tested at temperatures exceeding 1000 °C. Inspired by the findings of Mosher, Raj et al.,[21,22] Pezzotti et al.[23–27] have shown in detail how such an internal friction peak can be related to anelastic grain boundary sliding in high purity and in doped Si_3N_4 and SiC-based materials. Essentially, their theory relates the relative motion of neighbouring ceramic grains along their common grain boundary to the viscous properties and dimensions of the thin, amorphous, silicon oxynitride-based film, and to the elastic properties of the surrounding grains which impose limits to this relative motion. The temperature at which the grain boundary sliding (GBS-)peak occurs than is a function of a.o. the amount of amorphous grain boundary phase, but even more importantly, of the intrinsic grain boundary viscosity.

A second phenomenon giving rise to an internal friction peak in liquid-phase sintered ceramics, is described by Schaller et al., who have investigated silicon nitride ceramics containing substantial amounts of (Y,Al)-containing additives.[28–30] Schaller et al. have linked the appearance of an internal friction peak in these materials to the presence of an amorphous triple junction or pocket phase. Similar observations were made for zirconia ceramics.[31] The temperature at which this particular type of damping peak occurs is related to the glass transition of the amorphous phase. At temperatures sufficiently lower than the glass transition temperature (T_g) of the amorphous intergranular phase, the composite material consisting of a ceramic phase embedded in a glass, behaves in an elastic, low-damping manner. Upon heating, once the T_g of the glass phase is reached, the amorphous matter will behave in a viscous manner. Under cyclic loading the glass will therefore dissipate part of the periodically applied strain energy, particularly in glassy pockets in which the glass network is less constrained than in the thin grain boundary films. With increasing temperature, the glass viscosity will decrease, allowing for more viscous deformation in the small glass volumes, increasing the associated energy dissipation. Once the glass viscosity has reached too low a value for the glass to bear a relevant part of the applied load (a value which depends on the frequency of the applied cyclic load), less strain energy can be dissipated in the glass. That is when internal friction starts decreasing, until this glass transition (T_g-)damping peak reaches its high temperature foot.

Internal friction peaks, whether corresponding to the GBS- or the T_g-damping peak interpretations, are sensitive indicators of the presence of amorphous grain boundary phase, and allow a first prediction of its effect on the high temperature deformation resistance of the silicon nitride ceramic. Given the ressemblance of the silicon nitride materials tested by Schaller and the ones presented in this paper, one could be inclined to interpret the internal friction peaks in the SN-Y2Al4TiN2 and SN-Y2Al3TiN2 ceramics as T_g-peaks. In this case, the exponentially increasing 'background' damping (onto which the observed T_g-peaks are superimposed) can be the lower-temperature foot of the GBS-peak. If on the other hand the observed peak is of GBS nature, the background can be interpreted to be of a viscoplastic nature, indicating the onset of unrecoverable creep deformation. A conclusive distinction between GBS- and T_g-interpretations for the internal friction peaks observed in the SN-Y2Al4TiN2 and SN-Y2Al3TiN2 ceramics requires a more detailed study of the materials microstructure. However, irrespective of the particular micromechanistic origin, both GBS- and T_g-peak interpretations imply that the amount and effect of the amorphous grain boundary phase is more important in the SN-Y2Al4TiN2 and SN-Y2Al3TiN2 ceramics than in the other materials, for which, in the tested temperature and frequency range, no peaks were observed.

4.3. Stability of the intergranular amorphous phase after sintering

In the SN-Al5TiN4 and SN-Al6TiO4 ceramics, an Al–Ti–Si–O–N liquid phase is formed. A Y–Ti–Si–O–N melt is formed in the SN-Y6TiO_4 and SN-Y6TiO_{20} ceramics. Given the absence of an internal friction peak in the corresponding IET-spectra, we infer that upon cooling after sintering, the major part of the Y–Ti–Si–O–N and the Al–Ti–Si–O–N liquid phases devitrify. An Al–Si–O–N liquid phase is formed in the SN-Al4 ceramic. The extremely low internal friction in the SNAl4 material, containing an Al–Si–O–N liquid phase, combined with the absence of any secondary crystalline phase, suggests the latter is indeed mostly incorporated in the sialon phases. The liquid phase formed at the densification temperature in the SN-Y2Al4TiN2 and SN-Y2Al3TiN_2 ceramics is a Y–Al–Ti–Si–O–N melt. The Y–Al–Ti–Si–O–N melt does not devitrify (or partially at the most) and the remainder solidifies as a substantial amount of intergranular glass phase. The remarkable stability of the Y–Al–Ti–Si–O–N intergranular glass, i.e. its resistance to crystallisation, also during the high temperature IET tests (Fig. 3b), was reported previously.[14] The entrance of Ti-ions into the Y–Al–Si–O–N glass network was shown to stabilise this glass system.

4.4. Stability of the silicon (oxy-)nitride and titanium nitride phases

No significant changes in the volume fractions of the silicon (oxy-)nitride and titanium nitride phases can be discerned when after sintering the ceramics are investigated with HTXRD up to 1400 °C. However, surface effects do occur: the O-sialon phases formed in the SN-Y2Al4TiN2 and SN-Y2Al3TiN2 ceramics are not stable (e.g. Fig. 2a) especially in vacuum. In the SN-Al5TiN4, SN-Al6TiO4, SN-Y6TiO4, SN-Y6TiO20 and SN-Al4 ceramics, containing less amorphous intergranular phase, the O-sialon (or Si_2N_2O) phases are stable up to 1400 °C (Fig. 2b). These observations seem to indicate that the O-sialon phase dissolves in the Y–Al–Ti–Si–O–N intergranular glass phase between 1300 and 1400 °C.

Since the O-sialon instability concerns a surface effect, this explains why the internal friction peak during cooling is essentially the same as the peak during heating. The dissolution of silicon oxynitride in a (sub-)surface layer does not significantly increase the amount of intergranular amorphous phase of the 2 mm thick IET-sample.

The earlier observations and argumentation imply that, to use a silicon nitride-based composite containing the O-sialon (Si_2N_2O) phase at high temperature, and in reducing atmospheres, an intergranular glass phase must be avoided. This conclusion does not impede applications in oxidising atmospheres. Actually, Si_2N_2O is known to form in the subsurface layer of Si_3N_4-composites exposed to oxidation, thus reducing the degrading effects of oxidation.[32] Nevertheless, also in these circumstances, the intergranular glass phase will serve as an undesirable fast diffusion path.

4.5. Comparison of mechanical properties

The basic mechanical properties of all investigated ceramics are compared in Table 3. The best properties in terms of toughness are obtained for the ceramics, which did show an internal friction peak. This observation confirms the difficulty to find a compromise between high temperature performance and room temperature structural soundness: the presence of a substantial amount of amorphous phase is detrimental for the high temperature deformation resistance, but seems to be beneficial for fracture toughness.

Of all ceramics without a large amount of intergranular glass phase (i.e. of those ceramics with a more stable microstructure at elevated temperature), the SN-Y6TiO20 ceramic possesses the highest indentation toughness. For applications in which both toughness and high temperature stability are design parameters, this ceramic is judged most interesting of all tested materials. The microstructure of this ceramic—a high-TiN/high-Si_2N_2O/β-Si_3N_4 in-situ composite—is currently being further developed to obtain improved properties.

A particular observation can be made when comparing in more detail the indentation toughness values measured at room temperature with the internal friction values at elevated temperature. In Table 3, the internal friction measured at 1250 °C is given for each material. This temperature is chosen at the higher temperature-foot of the Q^{-1} peak observed in the materials with an amorphous pocket phase. The results in Table 3 suggest that there is a relation between high temperature internal friction (Q^{-1}) and room temperature indentation toughness (K_{IC}). If such relation truly exists, it must stem from a common micromechanical parameter. One candidate parameter is the grain boundary strength. A weak grain boundary facilitates grain boundary sliding and hence increases Q^{-1} at elevated temperature. Similarly, a weak grain boundary enables intergranular rather than transgranular crack growth, a requirement for high toughness. Another, related, but less direct explanation, can be the reduction of internal thermal stresses, which arise upon cooling after sintering. An increased amount of intergranular, low-melting amorphous material can postpone the genesis of these stresses during cooling. Further investigation is required to verify the soundness of these statements.

5. Conclusions

Si_3N_4–Si_2N_2O–TiN in-situ formed composites were successfully prepared by hot-pressing at 1650 °C. Internal friction measurements at elevated temperature revealed that five of seven prepared composites do not contain a substantial amount of amorphous intergranular glass phase. SN-Y2Al4TiN2 and SN-Y2Al3TiN2 ceramics do contain a substantial amount of intergranular glass phase, confirming the earlier reported stabilising effect of Ti-additives on intergranular amorphous Y–Si–Al–O–N phase. High-temperature X-ray diffraction shows that the silicon (oxy-)nitride and titanium nitride phases are compatible and stable up to 1400 °C. However, the silicon oxynitride phase is not stable above 1300 °C in a reducing environment in the presence of a substantial amount of intergranular glass phase. Long-term use of silicon oxynitride composites at elevated temepratures is hampered by the presence of an intergranular glass phase. The microstructure and properties of a high-TiN/high-Si_2N_2O/β-Si_3N_4 in-situ composite justify further efforts in its development to obtain improved properties.

Acknowledgements

R.G.D. thanks the academic board of the Katholieke Universiteit Leuven for a Junior Fellowship. G.R. thanks the Fund for Scientific Research (FWO)—Vlaanderen for his research fellowship.

References

1. Ekström, T. and Nygren, M., SiAlON ceramics. *J. Am. Ceram. Soc.*, 1992, **75**, 259–276.
2. Hoffmann, M. J., Geyer, A. and Oberacker, R., Potential of the sinter-hip-technique for the development of high-temperature resistant Si_3N_4-ceramics. *J. Eur. Ceram. Soc.*, 1999, **19**, 2359–2366.
3. Lewis, M. H., Crystallisation of grain boundary phases in silicon nitride and sialon ceramics. In *Tailoring of Mechanical Properties of Si_3N_4 Ceramics*, ed. M. J. Hoffmann and G. Petzow. Kluwer Academic Publishers, The Netherlands, 1994, pp. 217–231.
4. Trigg, M. B. and Jack, K. H., Solubility of aluminium in silicon oxynitride. *J. Mater. Sci. Letters*, 1987, **6**, 407–408.
5. Vleugels, J. and Van der Biest, O., Development, characterization and oxidation behaviour of Si_3N_4-Al_2O_3 ceramics. *J. Eur. Ceram. Soc.*, 1994, **13**, 529–544.
6. Wang, C. M., Emoto, H. and Mitomo, M., Nucleation and growth of silicon oxynitride grains in a fine-grained silicon nitride matrix. *J. Am. Ceram. Soc.*, 1998, **81**, 1125–1132.
7. Braue, W., Pleger, R. and Luxem, W., Nucleation and growth of Si_2N_2O in Si_3N_4 materials employing different sintering additives. *Key Eng. Mater.*, 1994, **89–91**, 483–488.
8. Sjoberg, J. and O'Meara, C., The effect of yttria additives on the composition of O-sialon prepared by pressureless sintering. *J. Eur. Ceram. Soc.*, 1992, **10**, 41–50.
9. Xu, Y., Huang, C. M., Kriven, W. M. and Zangvil, A., Residual α-Si_3N_4 in O-crystals in CeO_2-doped O + β SiAlON ceramics. *J. Am. Ceram. Soc.*, 1994, **77**, 2213–2216.
10. Hong, F., Lumby, R. J. and Lewis, M. H., TiN/sialon composites via in-situ reaction sintering. *J. Eur. Ceram. Soc.*, 1993, **11**, 237–239.
11. Ekström, T. and Olsson, P.-O., Beta-sialon ceramics with TiN particle inclusions. *J. Eur. Ceram. Soc.*, 1994, **13**, 551–559.
12. Lee, B.-T. and Kim, H.-D., In situ synthesis of TiN-reinforced Si_3N_4 matrix composites using Si and sponge Ti powders. *J. Mater. Sci.*, 1999, **34**, 6169–6171.
13. Wilhelm, M., Eder, C. and Wruss, W., Characterization of SiC- and TiN-particle-reinforced Si_3N_4 composites, *cfi/Ber. DKG, 2000, 25–28*.
14. Duan, R. G., Roebben, G., Vleugels, J. and Van der Biest, O., Stability of intergranular phases in hot-pressed Si_3N_4 studied with mechanical spectroscopy and in-situ high temperature XRD. *J. Eur. Ceram. Soc.*, 2002, **22**, 1897–1905.
15. ASTM E 1876–99, Am. Soc. Testing and Materials (2000).
16. Roebben, G., Bollen, B., Brebels, A., Van Humbeeck, J. and Van der Biest, O., Impulse excitation apparatus to measure resonant frequencies, elastic moduli, and internal friction at room and high temperature. *Rev. Sci. Instrum.*, 1997, **68**, 4511–4515.
17. Anstis, G. R., Chantikul, P., Lawn, B. R. and Marshall, D. B., A critical evaluation of indentation techniques for measuring fracture toughness: 1, direct crack measurements. *J. Am. Ceram. Soc.*, 1981, **64**, 533–538.
18. Hoffmann, M. J., High-temperature properties of Si_3N_4 ceramics. *MRS Bulletin*, 1995, **Feb**, 28–32.
19. Vetrano, J. S., Kleebe, H.-J., Hampp, E., Hoffmann, M. J. and Cannon, R. M., Epitaxial deposition of silicon nitride during post-sintering heat treatment. *J. Mater. Sci. Letters*, 1992, **11**, 1249–1252.
20. Chase, M. W. Jr. Davies, C. A., Downey, J. R. Jr. Frurip, D. J., Mcdonald, R. A., Syverud, A. N. In *JANAF Thermochemical Tables*, 3rd edn., ed. by D.R. Lide, Jr. American Chemical Society and American Institute of Physics for the National Bureau of Standard, MI, 1985.
21. Mosher, D. R. and Raj, R., Use of the internal friction technique to measure rates of grain boundary sliding. *Acta Metall.*, 1974, **22**, 1469–1474.
22. Mosher, D. R., Raj, R. and Kossowsky, R., Measurement of viscosity of the grain-boundary phase in hot-pressed silicon nitride. *J. Mater. Sci.*, 1976, **11**, 49–53.
23. Pezzotti, G., Ota, K. and Kleebe, H.-J., Grain-boundary relaxation in high-purity silicon nitride. *J. Am. Ceram. Soc.*, 1996, **79**, 2237–2246.
24. Pezzotti, G. and Ota, K., Grain-boundary sliding in fluorine-doped silicon nitride. *J. Am. Ceram. Soc.*, 1997, **80**, 599–603.
25. Pezzotti, G., Grain-boundary viscosity of Calcium-doped silicon nitride. *J. Am. Ceram. Soc.*, 1998, **81**, 2164–2168.
26. Pezzotti, G., Kleebe, H.-J., Okamoto, K. and Ota, K., Structure and viscosity of grain boundary in high-purity SiAlON ceramics. *J. Am. Ceram. Soc.*, 2000, **83**, 2549–2555.
27. Pezzotti, G., Wakasugi, T., Nishida, T., Ota, R., Kleebe, H.-J. and Ota, K., Chemistry and inherent viscosity of glasses segregated at grain boundaries of silicon nitride and silicon carbide ceramics. *J. Non-Crystalline Solids*, 2000, **271**, 79–87.
28. Lakki, A., Schaller, R., Bernard-Granger, G. and Duclos, R., High temperature anelastic behaviour of silicon nitride studied by mechanical spectroscopy. *Acta Metall. Mater.*, 1995, **43**, 419–426.
29. Donzel, L., Lakki, A. and Schaller, R., Glass transition and α relaxation in Y–Si–Al–O–N glasses and in Si_3N_4 ceramics studied by mechanical spectroscopy. *Philosophical Magazine*, 1997, **A**(76), 933–944.
30. Schaller, R., Mechanical spectroscopy of the high temperature brittle-to-ductile transition in ceramics and cermets. *J. Alloys Comp.*, 2000;7, **310**–15.
31. Donzel, L., Conforto, E. and Schaller, R., High-temperature mechanical spectroscopy of yttria-stabilized tetragonal zirconia polycrystals (Y-TZP) with different amounts of intergranular phase. *Acta Mater.*, 2000, **48**, 777–787.
32. Klemm, H., Herrmann, M. and Schubert, C., High temperature oxidation of silicon nitride based ceramics. In *Proc. 6th Intl Symp. on Ceramic Materials and Components for Engines, Arita, Japan*, ed. K. Niihara, S. Hirano, S. Kanzaki, K. Komeya and K. Morinaga; Wiley–VCH, Weinheim, Germany, 1998, pp. 576–581.